NEOPLASIA
www.neoplasia.com

Volume 15 Number 12 December 2013 pp. 1391–1399 1391

Combining Molecular Targeted Drugs to Inhibit Both Cancer Cells and Activated Stromal Cells in Gastric Cancer[1]

Mieko Onoyama*, Yasuhiko Kitadai*, Yuichiro Tanaka*, Ryo Yuge*, Kei Shinagawa†, Shinji Tanaka†, Wataru Yasui‡ and Kazuaki Chayama*

*Department of Gastroenterology and Metabolism, Graduate School of Biomedical and Health Sciences, Hiroshima University, Hiroshima, Japan; †Department of Endoscopy, Hiroshima University Hospital, Hiroshima, Japan; ‡Department of Molecular Pathology, Graduate School of Biomedical and Health Sciences, Hiroshima University, Hiroshima, Japan

Abstract

Recent studies have revealed that PDGF plays a role in promoting progressive tumor growth in several cancers, including gastric cancer. Cancer-associated fibroblasts, pericytes, and lymphatic endothelial cells in stroma express high levels of PDGF receptor (PDGF-R); cancer cells and vascular endothelial cells do not. Mammalian target of rapamycin (mTOR) is a serine/threonine kinase that increases the production of proteins that stimulate key cellular processes such as cell growth and proliferation, cell metabolism, and angiogenesis. In the present study, we examined the effects of PDGF-R tyrosine kinase inhibitor (nilotinib) and mTOR inhibitor (everolimus) on tumor stroma in an orthotopic nude mice model of human gastric cancer. Expression of PDGF-B and PDGF-Rβ mRNAs was associated with stromal volume. Treatment with nilotinib did not suppress tumor growth but significantly decreased stromal reactivity, lymphatic invasion, lymphatic vessel area, and pericyte coverage of tumor microvessels. In contrast, treatment with everolimus decreased tumor growth and microvessel density but not stromal reactivity. Nilotinib and everolimus in combination reduced both the growth rate and stromal reaction. Target molecule-based inhibition of cancer-stromal cell interaction appears promising as an effective antitumor therapy.

Neoplasia (2013) 15, 1391–1399

Introduction

In 2011, gastric cancer was reported as the world's fourth most common cancer in men and fifth most common in women [1]. The major cause of gastric cancer-associated mortality is metastasis. Recent studies in molecular and cellular biology have shown that tumor growth and metastasis are not determined by cancer cells alone but also by various stromal cells. The stroma constitutes a large part of most solid tumors, and the cancer-stromal cell interaction contributes functionally to tumor growth and metastasis [2,3]. Tumor stroma contains many different types of cells, including activated fibroblasts (myofibroblasts), endothelial cells, pericytes, and inflammatory cells. It has become clear that activated fibroblasts in cancer stroma are key modulators of tumor progression. As such, they are called cancer-associated fibroblasts (CAFs) [4]. Although the mechanisms that regulate activation of fibroblasts and their accumulation in tumors are not fully understood, PDGF, transforming growth factor β, and fibroblast growth factor 2 are known to be partly involved in this process [5].

PDGF and PDGF receptor (PDGF-R) are expressed in many human neoplasms, including prostate [6], lung [7], colon [8], and breast [9,10] neoplasms. We previously reported expression of PDGF-R in CAFs [11], pericytes, and lymphatic endothelial cells in the stroma of gastric cancer [12] but not in cancer cells or vascular

Abbreviations: CAF, cancer-associated fibroblast; mTOR, mammalian target of rapamycin; PDGF-R, PDGF receptor; VEGF, vascular endothelial growth factor

Address all correspondence to: Yasuhiko Kitadai, MD, PhD, Department of Gastroenterology and Metabolism, Graduate School of Biomedical and Health Sciences, Hiroshima University, 1-2-3 Kasumi, Minami-ku, Hiroshima 734-8551, Japan.
E-mail: kitadai@hiroshima-u.ac.jp

[1]This work was supported, in part, by grants-in-aid for Cancer Research from the Ministry of Education, Culture, Science, Sports, and Technology of Japan. The authors have no conflict of interest to report.
Received 20 September 2013; Revised 20 September 2013; Accepted 6 November 2013

DOI 10.1593/neo.131668

endothelial cells. PDGF-R signaling is reported to increase proliferation of tumor cells in an autocrine manner [13] and to stimulate angiogenesis [14], recruit pericytes [13,15], and control interstitial fluid pressure in stroma, influencing transvascular transport of chemotherapeutic agents in a paracrine manner [16]. Imatinib mesylate is a protein-tyrosine kinase inhibitor that was developed initially for its selectivity against breakpoint cluster region-Abelson (BCR-ABL) fusion protein [17]. The following additional tyrosine kinases are inhibited by imatinib: c-KIT, the receptor for KIT ligand (stem cell factor), two structurally similar PDGF-Rs (PDGF-Rα and PDGF-Rβ), and discoidin domain receptors (DDR1 and DDR2) [18,19]. Nilotinib has been established as a drug with potency superior to that of imatinib as an inhibitor of BCR-ABL. Nilotinib also inhibits the tyrosine kinase activity of the PDGF and c-KIT receptors DDR1 and DDR2 with efficacy similar that of imatinib [20,21].

The mammalian target of rapamycin (mTOR), a serine/threonine kinase, integrates multiple signaling pathways, including those that control growth and survival of tumor cells and angiogenesis. Mutations in upstream regulators of the mTOR signaling pathway, including epithelial growth factor receptor [22], phosphatidylinositol-3 kinase (PI3K) [22], and phosphatase and tensin homolog (PTEN) [23], have been frequently observed in human gastric cancer tissues. Phosphorylated mTOR, indicative of mTOR activation [24], has been positively correlated with tumor progression and poor survival in patients with gastric cancer [24,25]. mTOR exists in two complexes, mTORC1 and mTORC2 [26]. mTORC1 activation controls cell growth by regulating translation, ribosome biogenesis, autophagy, and metabolism [27]. mTORC2 phosphorylates Akt, serum/glucocorticoid regulated kinase 1 (SGK1), and protein kinase C to control multiple functions including cell survival and cytoskeletal organization [28]. mTOR also increases the translation of hypoxia-inducible factor 1α, which drives the expression of angiogenic growth factors such as vascular endothelial growth factor (VEGF), resulting in new vasculature. Everolimus is one of the rapalogs that inhibit mTORC1-mediated phosphorylation of S6 kinase 1 (S6K1) and 4E-binding protein 1 (4E-BP1), leading to decreased cell migration and invasion [29].

We examined, in an orthotopic nude mice model, whether nilotinib and everolimus have a synergic inhibitory effect on growth and metastasis of gastric cancer. We focused on cancer-stromal cell interactions because both the molecules and the cells targeted by these two drugs differ.

Materials and Methods

Human Gastric Cancer Cell Lines and Culture Conditions

Three gastric cancer cell lines, including high PDGF-B–expressing cells (TMK-1 and MKN-1) and low PDGF-B–expressing cells (KKLS), were used in this study [12]. The TMK-1 cell line (poorly differentiated adenocarcinoma) was kindly provided by Dr E. Tahara (Hiroshima University, Hiroshima, Japan). The MKN-1 cell line (adenosquamous carcinoma) was obtained from the Health Science Research Resources Bank (Osaka, Japan), and the KKLS cell line (undifferentiated carcinoma) was kindly provided by Dr Y. Takahashi (International University of Health and Welfare, Chiba, Japan). These cell lines were maintained in Dulbecco's Modified Eagle's Medium with 10% FBS (Sigma-Aldrich, St Louis, MO) and a penicillin-streptomycin mixture.

Animals and Orthotopic Implantation of Tumor Cells

Female athymic nude BALB/c mice were obtained from Charles River Japan (Tokyo, Japan). The mice were maintained under specific pathogen-free conditions and used at 5 weeks of age. The study was carried out after permission was granted by the Committee on Animal Experimentation of Hiroshima University. TMK-1, MKN-1, and KKLS cells were harvested from subconfluent cultures by brief exposure to 0.25% trypsin and 0.02% EDTA. Trypsinization was stopped with medium containing 10% FBS, and the cells were washed once in serum-free medium and resuspended in Hank's balanced salt solution. Only suspensions consisting of single cells with >90% viability were used. To produce gastric tumors, 1×10^6 cells in 50 μl of Hank's balanced salt solution were injected into the gastric wall of nude mice under observation with a zoom stereomicroscope (Carl Zeiss, Gottingen, Germany).

Treatment of Established Human Gastric Cancer Tumors Growing in the Gastric Wall of Nude Mice

To compare the therapeutic effects of imatinib and nilotinib on stromal cells, we performed preliminary experiments. The optimal biologic dose was used, as determined previously [30–32]. Seven days after the orthotopic implantation of TMK-1 or MKN-1 tumor cells, mice were randomized into the following three groups: those given water daily by oral gavage (control group), those given 50 mg/kg per day imatinib by oral gavage, and those given 50 mg/kg per day nilotinib by oral gavage. Treatments continued for 21 days, and the mice were killed on day 22. Excised tumors were subjected to immunohistochemistry.

To compare and evaluate the effect of combination therapy, 14 days after orthotopic implantation of TMK-1 tumor cells, mice were randomized to one of the following four treatments ($n = 6$ in each group): 1) daily oral gavage of water (control group), 2) daily oral gavage of nilotinib (100 mg/kg; nilotinib group), 3) daily oral gavage of everolimus (2 mg/kg; everolimus group), and 4) daily oral gavage of nilotinib (100 mg/kg) and everolimus (2 mg/kg; combination group). Combination studies with imatinib and everolimus were not performed due to drug-drug interactions that effect the pharmacokinetic profiles and tolerability of the agents *in vivo*. The mice were treated for 35 days, and then killed and subjected to necropsy.

Necropsy Procedures and Histologic Studies

Mice bearing orthotopic tumors were killed by diethyl ether. Body weights were recorded. After necropsy, tumors were excised and weighed. For immunohistochemistry, one part of the tumor tissue was fixed in formalin-free IHC Zinc Fixative (BD Pharmingen, San Diego, CA) and embedded in paraffin, and the other part was embedded in OCT Compound (Miles Laboratories, Elkhart, IN), rapidly frozen in liquid nitrogen, and stored at −80°C. All macroscopically enlarged regional (celiac and para-aortal) lymph nodes were harvested, and the presence of metastatic disease was confirmed by histologic examination.

Patients and Tumor Specimens

To examine the clinical importance of PDGF/receptor signaling and mTOR signaling, endoscopic biopsy or surgical specimens were obtained from 29 patients with gastric cancer who underwent surgical resection at Hiroshima University Hospital. The specimens were examined by quantitative RT-PCR (RT-PCR) and immunohistochemistry, respectively. The biopsy specimens were snap frozen in

liquid nitrogen and stored at −80°C until RNA extraction. Use of the specimens was in accordance with the Ethical Guidelines for Human Genome/Gene Research of the Japanese Government. Patient informed consent was not required, but identifying information for all samples was removed before analysis.

Quantitative RT-PCR Analysis

Total RNA was extracted from the gastric cancer cell lines and biopsy specimens with an RNeasy Kit (Qiagen, Valencia, CA) according to the manufacturer's instructions. cDNA was synthesized from 1 μg of total RNA with a first-strand cDNA synthesis kit (Amersham Biosciences, Piscataway, NJ). After reverse transcription of RNA into cDNA, quantitative RT-PCR was performed with a LightCycler FastStart DNA Master SYBR Green I kit (Roche Diagnostics, Basel, Switzerland) according to the manufacturer's recommended protocol. Reactions were carried out in triplicate. To correct for differences in both RNA quality and quantity between samples, values were normalized to those of glyceraldehyde-3-phosphate dehydrogenase (GAPDH). The mRNA ratio between gastric carcinoma tissues (T) and corresponding normal mucosa (N) was calculated and expressed as the T/N ratio. Primers for PCR were designed with specific primer analysis software (Primer Designer; Scientific and Educational Software, Cary, NC), and specificity of the sequences was confirmed by FASTA [European Molecular Biology Laboratory (EMBL) Database, Heidelberg, Germany]. Respective primer sequences, annealing temperatures, and PCR cycles were as previously reported [12].

Reagents

Imatinib (Gleevec), nilotinib (Tasigna), and everolimus (Afinitor) were kindly provided by Novartis Pharma (Basel, Switzerland). Imatinib and everolimus were diluted in sterile water for oral administration. Nilotinib was disolved in 0.5% hydroxypropylmethylcellulose aqueous solution containing 0.05% Tween 80 at the concentration of 4 mg/ml and then diluted in sterile water. Primary antibodies were purchased as follows: polyclonal rabbit anti–PDGF-Rβ, polyclonal rabbit antiphosphorylated PDGF-Rβ (p–PDGF-Rβ), and polyclonal rabbit anti-human VEGF-A (sc-152) from Santa Cruz Biotechnology (Santa Cruz, CA); rat anti-mouse CD31 [(platelet endothelial cell adhesion molecule (PECAM1)] from BD Pharmingen; mouse anti-desmin monoclonal antibody from Molecular Probes (Eugene, OR); rabbit anti–α-smooth muscle actin (α-SMA; ab5694) from Abcam (Cambridge, United Kingdom); Ki-67–equivalent antibody (MIB-1) from Dako (Carpinteria, CA); monoclonal rat anti-mouse lymphatic vessel endothelial hyaluronan receptor 1 (Lyve-1) antibody from R&D Systems (Minneapolis, MN); polyclonal rabbit anti-mouse type I collagen from Novotec (Saint Martin La Garenne, France); and monoclonal rabbit anti-mouse S6 ribosomal protein antibody (No. 2217) and monoclonal rabbit antiphosphorylated mouse S6 ribosomal protein antibody (No. 4858) from Cell Signaling Technology (Beverly, MA). The following fluorescent secondary antibodies were used: Alexa 488-conjugated goat anti-rabbit IgG, Alexa 488-conjugated goat anti-rat IgG, and Alexa 546-conjugated goat anti-rabbit IgG (all from Molecular Probes).

Immunofluorescence for PDGF-Rβ and p–PDGF-Rβ and Double Immunofluorescence for CD31 (Vascular Endothelial Cells) and Desmin (Pericytes)

Fresh-frozen specimens of TMK-1 human gastric cancer tissue obtained from nude mice were cut into 8-μm sections and mounted on positively charged slides. After fixation with ice-cold acetone for 20 minutes, washing and blocking were performed as previously described [11]. The slides were incubated for 3 hours at room temperature with primary antibody against PDGF-Rβ or p–PDGF-Rβ. Slides were incubated for 1 hour at room temperature with Alexa 546-conjugated goat anti-rabbit IgG secondary antibody and then nuclear counterstained with 4′,6-diamidino-2-phenylindole (DAPI) for 10 minutes. PDGF-Rβ or p–PDGF-Rβ was identified by red fluorescence.

For double immunofluorescence, after fixation, washing, and blocking, the slides were incubated overnight at 4°C with Fab fragment goat anti-mouse IgG (Jackson ImmunoResearch Laboratories, West Grove, PA) to block endogenous immunoglobulins. Then, slides were incubated with the primary antibody desmin for 3 hours at room temperature. This was followed by incubation for 1 hour at room temperature with Alexa 546-conjugated goat anti-mouse IgG secondary antibody. Slides were then incubated for 3 hours at room temperature with antibody against CD31 and incubated for 1 hour at room temperature with Alexa 488-conjugated goat anti-rat IgG secondary antibody. The samples were then nuclear counterstained with DAPI. Endothelial cells were identified by green fluorescence, whereas pericytes were identified by red fluorescence. The coverage of pericytes on endothelial cells was determined by counting CD31-positive cells in direct contact with desmin-positive cells in five randomly selected microscopic fields (at ×200 magnification) [33].

Confocal Microscopy

Confocal fluorescence images were obtained with the use of a ×20 or ×40 objective lens on a Carl Zeiss LSM laser scanning microscopy system (Carl Zeiss Inc, Thornwood, NY).

Immunohistochemistry and Terminal Deoxynucleotide Transferase-Mediated dUTP-Biotin Nick End Labeling

Immunohistochemistry for α-SMA, type I collagen, Ki-67, Lyve-1, phosphorylated S6 ribosomal protein, or VEGF-A was performed on formalin-free zinc-fixed, paraffin-embedded tissues cut into serial 4-μm sections. After deparaffinization and rehydration, tissue sections to be stained for α-SMA, type I collagen, Ki-67, Lyve-1, phosphorylated S6 ribosomal protein, or VEGF-A were pretreated by microwaving them twice for 5 minutes in Dako REAL Target Retrieval Solution (Dako). Primary antibodies were applied to the slides and incubated overnight in humidified boxes at 4°C. After incubation for 1 hour at room temperature with corresponding peroxidase-conjugated secondary antibodies, a positive reaction was detected by exposure to stable DAB for 5 to 10 minutes. Slides were counterstained with hematoxylin for visualization of the nucleus. Apoptotic cells in tissue sections were detected by terminal deoxynucleotide transferase-mediated deoxyuridine triphosphates (dUTP)-biotin nick end labeling (TUNEL) assay with the ApopTag Plus Peroxidase *In Situ* Apoptosis Detection Kit (Chemicon Intl, Temecula, CA) according to the manufacturer's instructions.

Quantification of the CAF (α-SMA–Positive), Collagen (Type I Collagen-Positive), Microvessel (CD31-Positive), and Lymphatic Vessel (Lyve-1–Positive) Areas

To evaluate angiogenic and lymphangiogenic activity of the tumors, the areas of vascular and lymphatic microvessels were quantified. Ten random fields at ×200 (for vascular microvessels) or ×100 (for lymphatic microvessels) magnification were captured for each tumor, and the outline of each vascular or lymphatic microvessel including a lumen was manually traced. The areas were then calculated with

the use of National Institutes of Health ImageJ software (Wayne Rasband, Bethesda, MD). The areas of CAFs and extracellular matrix (ECM) were also determined from the respective areas of α-SMA–positive and type I collagen-positive staining from 10 optical fields (original magnification, ×100) of different sections.

Determination of the Ki-67 Labeling Index and the Apoptotic Index

The Ki-67 labeling index (Ki-67 LI) was determined by light microscopy at the site of the greatest number of Ki-67–positive cells. Cells were counted in 10 fields at ×200 magnification, and the number

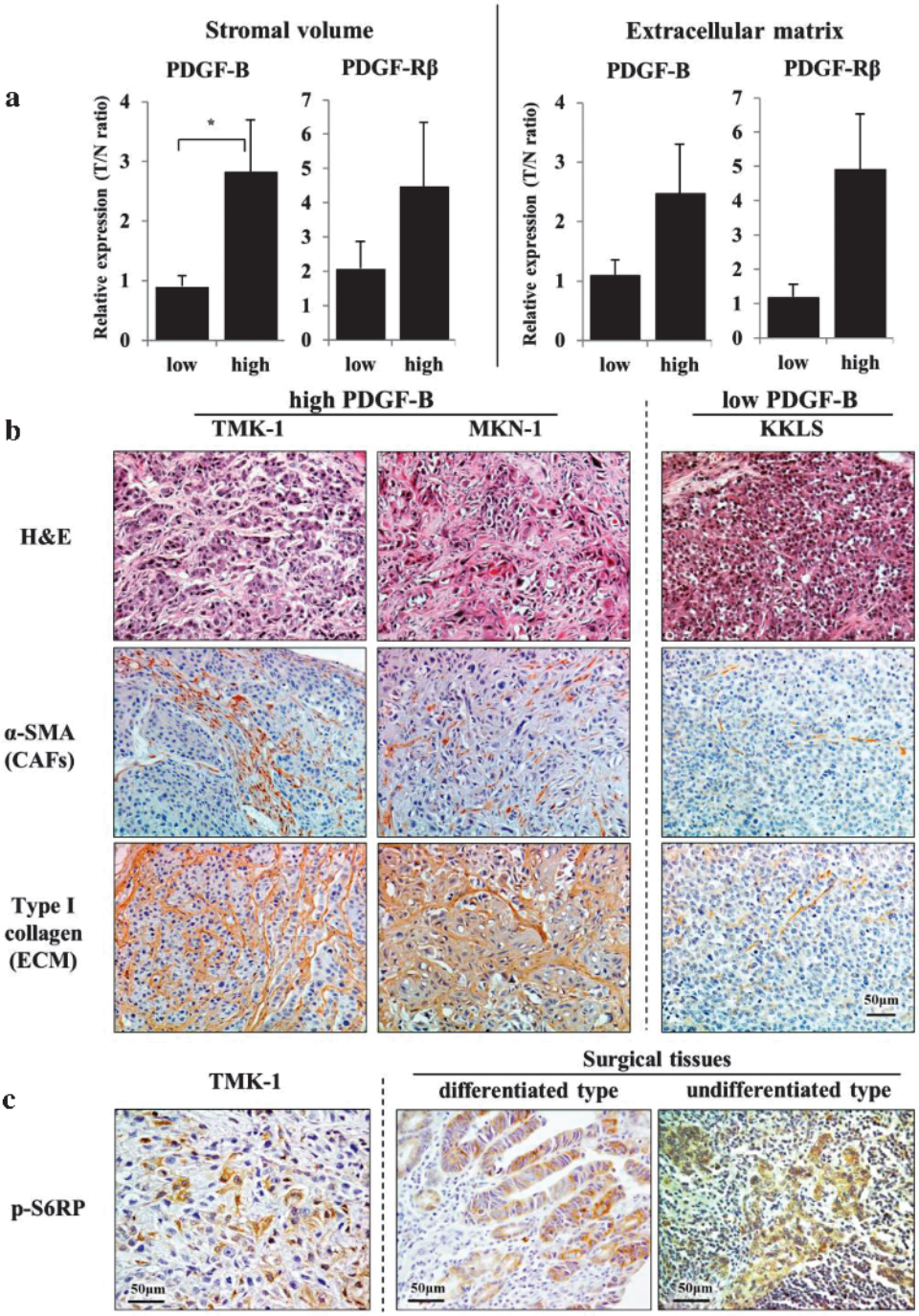

Figure 1. Expression of PDGF-B and PDGF-Rβ mRNAs in relation to stromal volume and ECM production in human gastric cancer tissues (A). Stromal volume and ECM production were evaluated by immunostaining for α-SMA and type I collagen, respectively. Tissues were classified as those with low (below median value) and those with high (higher than median value) expression levels. T/N ratio is the ratio of expression in cancer tissue to that of normal mucosa. The bars represent means + SE. *$P < .05$. Hematoxylin and eosin (H&E) staining and immunohistochemistry for α-SMA and type I collagen in orthotopic xenografts (B). Tumors with high PDGF-B mRNA expression (TMK-1 and MKN-1 tumors) have rich stroma, whereas tumors with low PDGF-B mRNA expression (KKLS tumors) have scanty stroma. CAFs are cancer-associated fibroblasts. Immunohistochemistry for p-S6RPs in primary gastric cancer tissue (C). Expression of p-S6RP is detected in cytoplasm of cancer cells in TMK-1 orthotopic tumor and in differentiated and undifferentiated human gastric cancers.

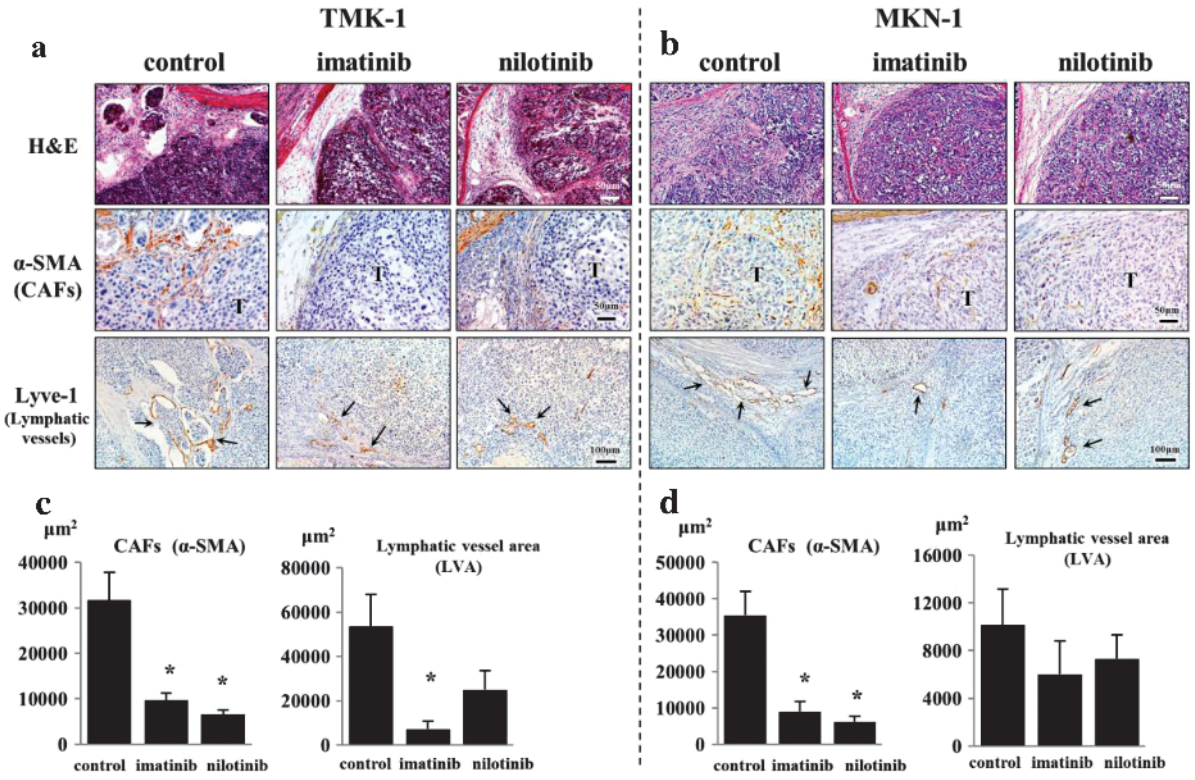

Figure 2. Effects of imatinib and nilotinib on stroma of TMK-1 and MKN-1 tumors. H&E staining and immunohistochemistry for α-SMA and Lyve-1 in TMK-1 (A) and MKN-1 (B) orthotopic tumors are shown. The stromal reaction (evaluated by immunostaining for α-SMA) was significantly reduced in mice treated with imatinib and nilotinib in comparison to that in control group mice (C and D). Lymphatic vessel area (Lyve-1–positive area) decreased especially in the group of mice with TMK-1 tumors treated with imatinib and nilotinib (C and D). T, tumor nest; arrows, dilated lymphatic vessels. *$P < .05$; bars, SE.

of positive cells among approximately 300 tumor cells was counted and expressed as a percentage. The number of apoptotic cells was counted in 10 random 0.14-mm^2 fields at ×200 magnification. The apoptotic index was taken as the ratio of positively stained tumor cells and bodies to all tumor cells and expressed as a percentage for each case.

Statistical Analysis

Values are expressed as means ± SE. Between-group differences in murine body weight, tumor weight, and the areas of α-SMA–positive, type I collagen-positive, CD31-positive, and Lyve-1–positive cells were analyzed by Wilcoxon/Kruskal-Wallis test. Differences in the incidence of lymph node metastasis were analyzed by Fisher's exact test. Differences in the percentages of Ki-67–positive cells and TUNEL-positive cells were analyzed by unpaired Student's t test or χ^2 test as appropriate. A P value of <.05 was considered statistically significant.

Results

Expression of PDGF-B and PDGF-Rβ in Relation to Stromal Reaction in Human Gastric Cancers

We first examined mRNA expression levels of PDGF-B and PDGF-Rβ in relation to stromal reaction in human gastric cancer tissues. Stromal reaction was evaluated as stromal volume and as ECM production by immunohistochemistry for α-SMA and type I collagen, respectively (Figure 1*A*). Stromal volume was significantly higher in the PDGF-B–high group than in the PDGF-B–low group. ECM production tended to be greater in the PDGF-B–high group. PDGF-Rβ expression was clearly related to stromal reaction.

TMK-1 and MKN-1 cells (high PDGF-B–expressing cells) produced orthotopic tumors with abundant stroma; however, KKLS cells (low PDGF-B–expressing cells) did not (Figure 1*B*). Thus, the PDGF/receptor system may be involved in tumor–stromal cell interaction.

Table 1. Effects of Nilotinib and Everolimus on Orthotopic TMK-1 Tumors per Treatment Group.

Group	Body Weight (g)	Tumor Incidence	Tumor Weight (g)	Lymph Node Metastasis
Control	21.8 (17.8-24.6)	5/5	0.33 (0.07-0.72)	3/5
Nilotinib (100 mg/kg)	20.6 (18.5-23.5)	5/5	0.35 (0.10-0.45)	4/5
Everolimus (2 mg/kg)	22.0 (20.4-23.9)	4/6	0.08 (0.00-0.15)*	3/6
Nilotinib (100 mg/kg) + everolimus (2 mg/kg)	21.3 (16.3-22.1)	1/6	0.006 (0.00-0.04)†	0/6

Control group ($n = 5$), nilotinib group ($n = 5$), everolimus group ($n = 6$), and nilotinib plus everlimus group ($n = 6$).
Ranges are shown in parentheses.
*$P < .05$ *versus* control group values.
†$P < .01$ *versus* control group values.

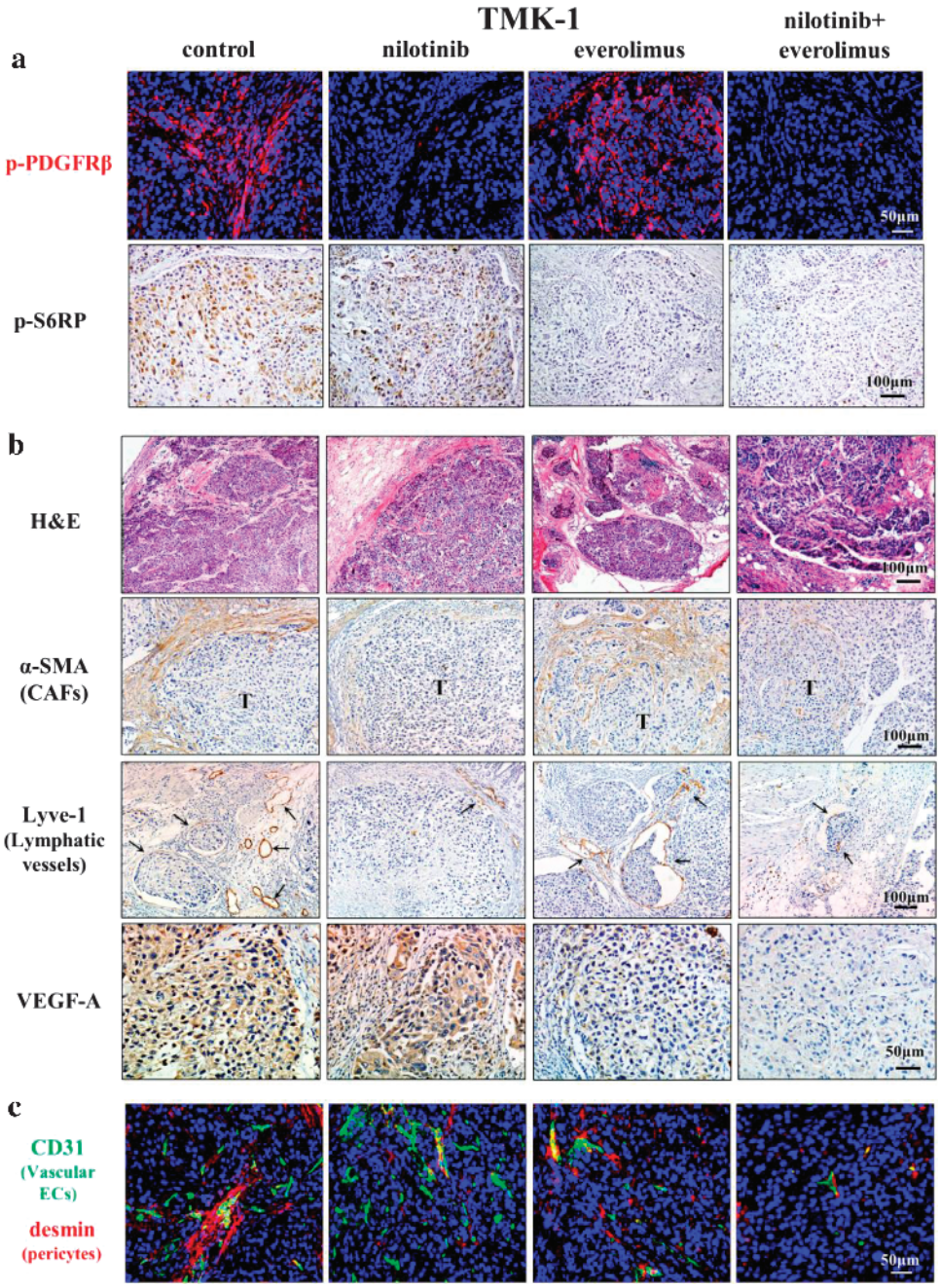

Figure 3. Effects of nilotinib and/or everolimus on TMK-1 orthotopic tumors. Phosphorylation of downstream target protein for nilotinib and everolimus. Treatment with nilotinib inhibited expression of p–PDGF-Rβ. Treatment with everolimus inhibited phosphorylation of S6RP (A). H&E and immunohistochemical staining for α-SMA, Lyve-1, and VEGF-A in TMK-1 orthotopic gastric tumor (B). Effects of nilotinib and everolimus on microvessels in TMK-1 tumor. Pericyte coverage on tumor-associated endothelial cells in the TMK-1 gastric tumors (C). Treatment with nilotinib reduced pericyte coverage of microvessels. Vascular endothelial cells were identified by green fluorescence, whereas desmin (pericytes) were identified by red fluorescence.

Activation of mTOR Signaling Pathway in Human Gastric Cancers

We next examined activation of the mTOR pathway in human gastric cancer tissues obtained surgically. Phosphorylation of S6 (p-S6) ribosomal proteins (p-S6RP) was assessed to evaluate activity of the mTOR signaling pathway. In all 29 human gastric cancers, tumor cells were shown by immunohistochemistry to express p-S6RP. Although expression of p-S6RP was detected in both differentiated and undifferentiated gastric cancers (Figure 1*C*), the staining was heterogeneous; that is, it was weak at the invasive edge (staining not shown). Tumor cells in xenografts implanted into nude mice were also positive for p-S6RP (Figure 1*C*).

Effects of Imatinib and Nilotinib on Tumor Stroma

In the first set of animal experiments, we examined the effects of PDGF-R tyrosine kinase inhibitors, imatinib and nilotinib, on stroma of TMK-1 and MKN-1 tumors. The stromal reaction at the tumor

periphery was significantly reduced in mice treated with imatinib or nilotinib in comparison to that in control mice (Figure 2, *A* and *B*). A decrease in the lymphatic vessel area (Lyve-1–positive area) was also noted, especially in the TMK-1 tumors of mice treated with both imatinib and nilotinib (Figure 2, *A* and *C*).

Combining Treatment of Human Gastric Cancer Growing in the Gastric Wall of Nude Mice

We next determined whether nilotinib and everolimus, administered in combination, have a synergistic effect. The growth and metastasis of TMK-1 human gastric cancer cells implanted in the gastric wall of nude mice were evaluated. The tumor incidence was 100% in all treatment groups. Toxicity of the various treatment regimens was assessed on the basis of change in body weight. Oral administration of nilotinib, everolimus, and of the two drugs in combination did not significantly affect body weight (Table 1). Tumor growth and metastasis were not inhibited in mice treated with nilotinib alone (*vs* control mice); however, tumor growth was significantly inhibited in mice treated with everolimus alone. Furthermore, tumor growth was much more inhibited with the combination treatment. In five of six mice, tumors were not detected macroscopically. Lymph node metastasis was significantly inhibited only in mice treated with nilotinib and everolimus in combination (Table 1).

Histopathologic Analysis of TMK-1 Tumors

To assess whether nilotinib and everolimus inhibit targeted molecules, tumor sections were analyzed immunohistochemically for the expression of p–PDGF-Rβ and p-S6RP. The phosphorylation of PDGF-Rβ was significantly inhibited in orthotopic tumors of mice treated with nilotinib alone or with nilotinib and everolimus in combination (Figure 3*A*). The phosphorylation of S6 ribosomal protein was significantly inhibited in orthotopic tumors of mice treated with everolimus alone or nilotinib and everolimus in combination (Figure 3*A*).

The periphery of TMK-1 gastric tumors was adjacent to abundant stroma, into which tumor cells infiltrated. In contrast, gastric tumors in mice treated with nilotinib alone or with nilotinib and everolimus in combination were surrounded by scanty stroma (Figure 3*B* and Table 2). In addition, treatment with everolimus alone or with nilotinib and everolimus in combination significantly reduced the areas of vascular microvessels (Table 2), although treatment with nilotinib alone or with nilotinib and everolimus in combination significantly reduced the number of lymphatic vessels (Figure 3*B* and Table 2). The number of pericytes covering endothelial cells was also decreased (Figure 3*C* and Table 2).

Proliferation of tumor cells was evaluated by staining for Ki-67. The control group Ki-67 LI (39.6 ± 5.2) was significantly decreased with treatment by combination treatment (13.1 ± 2.3; $P < .01$; Table 2).

According to TUNEL assay, the median number of apoptotic tumor cells in control mice was 6.94 ± 1.26. The number of apoptotic cells in tumors of mice from each of the groups treated with everolimus was significantly increased in comparison to the number in control mice (Table 2).

mTOR Inhibitor Reduced Expression of VEGF-A

Treatment with everolimus or nilotinib and everolimus in combination inhibited the number and area of vascular microvessels. Therefore, we examined expression of angiogenic factor VEGF-A. Immunoreactivity of VEGF-A in tumor cells was markedly suppressed by treatment with everolimus (Figure 3*B*).

Discussion

In the present study, treatment with imatinib or nilotinib (PDGF-R tyrosine kinase inhibitor) significantly reduced the stromal reaction, area of lymphatic vessels, and pericyte coverage, consistent with our previously reported findings [11,12]. However, tumor growth and microvessel density were not inhibited. In contrast, treatment with everolimus (mTOR inhibitor) induced apoptosis of tumor cells and inhibited angiogenesis but did not influence the stromal reaction. More interestingly, nilotinib and everolimus administered in combination dramatically inhibited tumor growth, angiogenesis, stromal reaction, and lymph node metastasis. Primary tumors were not detected in five of six mice, and no lymph node metastasis was found in any of the mice in the combination drug group.

Imatinib and nilotinib are well-known multiple tyrosine kinase inhibitors that inhibit mainly BCR-ABL, c-KIT, DDR1, DDR2, and PDGF-Rs. BCR-ABL and c-KIT are not expressed in gastric cancer cells (data not shown). DDRs have been reported to be activated by different types of collagen and participate in several processes such as cell adhesion, migration, and proliferation [34]. So far, there is no report concerning the role of DDRs in human gastric cancer. We reported previously that PDGF ligands are expressed by gastric cancer cells, whereas PDGF-Rs are expressed mainly by stromal cells [12].

Table 2. Immunohistochemical Analysis of TMK-1 Human Gastric Carcinoma Cells per Treatment Group.

Group	Tumor Cells		Vascular Endothelial Cells			Lymphatic Endothelial Cells
	Ki-67 LI* (%)	TUNEL† (%)	MVC‡ (Per Field)	MVA§ (/× 10^3 μm^2)	Pericyte Coverage¶ (%)	LVA# (/× 10^3 μm^2)
Control	39.64 ± 5.24	6.94 ± 1.26	11.2 ± 1.48	6.90 ± 0.84	61.8 ± 9.89	81.50 ± 16.51
Nilotinib (100 mg/kg)	35.87 ± 1.75	6.82 ± 0.68	10.9 ± 0.82	4.34 ± 0.70**	31.8 ± 3.87**	7.21 ± 0.89††
Everolimus (2 mg/kg)	31.30 ± 4.54	13.8 ± 1.07††	6.5 ± 0.50**	1.66 ± 0.29††	57.8 ± 7.83	51.63 ± 10.23
Nilotinib (100 mg/kg) + everolimus (2 mg/kg)	13.15 ± 2.30††	11.0 ± 1.57**	7.2 ± 0.38	1.26 ± 0.14††	16.2 ± 4.98**	0.84 ± 0.37††

Ki-67 LI, Ki-67 labeling index; MVC, microvessel count; MVA, microvessel area; LVA, lymphatic vessel area.
Control mice were given water daily by oral gavage. Control group ($n = 5$), nilotinib group ($n = 5$), everolimus group ($n = 6$), and nilotinib and everlimus group ($n = 6$).
*Number (mean ± SE) of Ki-67–positive tumor cells per field determined by measuring 10 random 0.14-mm^2 fields at ×200 magnification.
†Percentage of TUNEL-positive tumor cells (out of total number of cells) per 0.14-mm^2 fields at ×200 magnification.
‡MVC was determined by counting 10 random fields at ×200 magnification.
§MVA was determined by measuring 10 random fields at ×200 magnification.
¶CD31-positive cells in direct contact with desmin-positive cells were counted in five random fields at ×200 magnification.
#LVA was determined by measuring 10 random fields at ×100 magnification.
**$P < .05$ *versus* control group values.
††$P < .01$ *versus* control group values.

Therefore, blockade of PDGF-R signaling by imatinib or nilotinib may decrease the stromal reaction, areas of lymphatic vessels, and number of pericytes. Inhibition of PDGF-Rβ phosphorylation in stromal cells was confirmed by immunofluorescence in the present study.

Everolimus is a rapalog, one of the mTOR inhibitors. The best characterized cellular effect of rapamycin on tumor cells is the growth retardation by cell cycle arrest in G_1 phase of the cell cycle [35]. Treatment with rapamycin at high concentrations results in an accumulation of cells in S phase and induction of apoptosis in certain cell systems [36]. Rapamycin is reported to reduce the production of VEGF by tumor cells and block VEGF-mediated stimulation of endothelial cells and tube formation [37]. Therefore, rapamycin administration can induce apoptosis of VEGF-stimulated endothelial cells, potentially leading to tumor vessel thrombosis [38]. These effects of rapamycin match our findings that treatment with everolimus induced apoptosis and inhibited VEGF expression of tumor cells.

The effects of rapamycin on lymphangiogenesis and lymph node metastasis were recently investigated in a nude mice model, and rapamycin significantly reduced the number and area of lymphatic vessels in the primary tumor [39,40]. Lymph node metastasis was significantly suppressed in the rapamycin-treated nude mice. The VEGF-C/vascular endothelial growth factor receptor-3 (VEGFR-3) signal transduction pathway plays a causal role in tumor-associated lymphangiogenesis and lymphatic metastasis [41]. Rapamycin repressed protein and mRNA expressions of VEGF-A and VEGF-C in B13LM cells under both serum-starved and normal culture conditions [40], suggesting that rapamycin inhibits lymphangiogenesis *in vivo* probably by inhibition of VEGF-C expression. Rapamycin also impairs downstream signaling of VEGF-A and VEGF-C through the mTOR/S6K1 pathway in lymphatic endothelial cells [39]. In our mouse model, inhibition of lymphangiogenesis was observed under treatment with nilotinib but not everolimus. Further studies are needed to determine whether everolimus inhibits lymphangiogenesis.

Rapalogs in combination with other anticancer agents, including standard chemotherapy agents, receptor tyrosine kinase–targeted agents, and angiogenesis inhibitors, have shown greater activity than single-agent rapalog, suggesting that rapalogs may be best used in combination therapies [42]. However, the mechanisms of increased efficacy have not been elucidated. The present study showed that PDGF-R inhibitor and rapalog inhibited activated stromal components and neoplastic cells, respectively. Combination therapy based on these drugs may block cancer-stromal interaction, and mTOR inhibitor appears promising as a therapeutic agent against stromal compartment–rich tumors.

Acknowledgments

The authors thank Shinichi Norimura for his excellent technical assistance. This work was carried out with the kind cooperation of the Analysis Center of Life Science and Institute of Laboratory Animal Science, Hiroshima University, and we thank Novartis Pharma KK for providing the imatinib, nilotinib, and everolimus.

References

[1] Jemal A, Bray F, Center MM, Ferlay J, Ward E, and Forman D (2011). Global cancer statistics. *CA Cancer J Clin* **61**, 69–90.

[2] Mantovani A, Allavena P, Sica A, and Balkwill F (2008). Cancer-related inflammation. *Nature* **454**, 436–444.

[3] Whiteside TL (2008). The tumor microenvironment and its role in promoting tumor growth. *Oncogene* **27**, 5904–5912.

[4] Mueller MM and Fusenig NE (2004). Friends or foes—bipolar effects of the tumour stroma in cancer. *Nat Rev Cancer* **4**, 839–849.

[5] Kitadai Y (2010). Cancer-stromal cell interaction and tumor angiogenesis in gastric cancer. *Cancer Microenviron* **3**, 109–116.

[6] Uehara H, Kim SJ, Karashima T, Shepherd DL, Fan D, Tsan R, Killion JJ, Logothetis C, Mathew P, and Fidler IJ (2003). Effects of blocking platelet-derived growth factor-receptor signaling in a mouse model of experimental prostate cancer bone metastases. *J Natl Cancer Inst* **95**, 458–470.

[7] Antoniades HN, Galanopoulos T, Neville-Golden J, and O'Hara CJ (1992). Malignant epithelial cells in primary human lung carcinomas coexpress *in vivo* platelet-derived growth factor (PDGF) and PDGF receptor mRNAs and their protein products. *Proc Natl Acad Sci USA* **89**, 3942–3946.

[8] Lindmark G, Sundberg C, Glimelius B, Påhlman L, Rubin K, and Gerdin B (1993). Stromal expression of platelet-derived growth factor beta-receptor and platelet-derived growth factor B-chain in colorectal cancer. *Lab Invest* **69**, 682–689.

[9] Seymour L, Dajee D, and Bezwoda WR (1993). Tissue platelet derived-growth factor (PDGF) predicts for shortened survival and treatment failure in advanced breast cancer. *Breast Cancer Res Treat* **26**, 247–252.

[10] Yi B, Williams PJ, Niewolna M, Wang Y, and Yoneda T (2002). Tumor-derived platelet-derived growth factor-BB plays a critical role in osteosclerotic bone metastasis in an animal model of human breast cancer. *Cancer Res* **62**, 917–923.

[11] Sumida T, Kitadai Y, Shinagawa K, Tanaka M, Kodama M, Ohnishi M, Ohara E, Tanaka S, Yasui W, and Chayama K (2011). Anti-stromal therapy with imatinib inhibits growth and metastasis of gastric carcinoma in an orthotopic nude mouse model. *Int J Cancer* **128**, 2050–2062.

[12] Kodama M, Kitadai Y, Sumida T, Ohnishi M, Ohara E, Tanaka M, Shinagawa K, Tanaka S, Yasui W, and Chayama K (2010). Expression of platelet-derived growth factor (PDGF)-B and PDGF-receptor β is associated with lymphatic metastasis in human gastric carcinoma. *Cancer Sci* **101**, 1984–1989.

[13] Ostman A (2004). PDGF receptors-mediators of autocrine tumor growth and regulators of tumor vasculature and stroma. *Cytokine Growth Factor Rev* **15**, 275–286.

[14] Risau W, Drexler H, Mironov V, Smits A, Siegbahn A, Funa K, and Heldin CH (1992). Platelet-derived growth factor is angiogenic *in vivo*. *Growth Factors* **7**, 261–266.

[15] Bergers G, Song S, Meyer-Morse N, Bergsland E, and Hanahan D (2003). Benefits of targeting both pericytes and endothelial cells in the tumor vasculature with kinase inhibitors. *J Clin Invest* **111**, 1287–1295.

[16] Pietras K (2004). Increasing tumor uptake of anticancer drugs with imatinib. *Semin Oncol* **31**, 18–23.

[17] Druker BJ and Lydon NB (2000). Lessons learned from the development of an abl tyrosine kinase inhibitor for chronic myelogenous leukemia. *J Clin Invest* **105**, 3–7.

[18] Fletcher JA (2004). Role of KIT and platelet-derived growth factor receptors as oncoproteins. *Semin Oncol* **31**, 4–11.

[19] Day E, Waters B, Spiegel K, Alnadaf T, Manley PW, Buchdunger E, Walker C, and Jarai G (2008). Inhibition of collagen-induced discoidin domain receptor 1 and 2 activation by imatinib, nilotinib and dasatinib. *Eur J Pharmacol* **599**, 44–53.

[20] Weisberg E, Manley PW, Breitenstein W, Brüggen J, Cowan-Jacob SW, Ray A, Huntly B, Fabbro D, Fendrich G, Hall-Meyers E, et al. (2005). Characterization of AMN107, a selective inhibitor of native and mutant Bcr-Abl. *Cancer Cell* **7**, 129–141.

[21] Manley PW, Stiefl N, Cowan-Jacob SW, Kaufman S, Mestan J, Wartmann M, Wiesmann M, Woodman R, and Gallagher N (2010). Structural resemblances and comparisons of the relative pharmacological properties of imatinib and nilotinib. *Bioorg Med Chem* **18**, 6977–6986.

[22] Corso G, Velho S, Paredes J, Pedrazzani C, Martins D, Milanezi F, Pascale V, Vindigni C, Pinheiro H, Leite M, et al. (2011). Oncogenic mutations in gastric cancer with microsatellite instability. *Eur J Cancer* **47**, 443–451.

[23] Wen YG, Wang Q, Zhou CZ, Qiu GQ, Peng ZH, and Tang HM (2010). Mutation analysis of tumor suppressor gene *PTEN* in patients with gastric carcinomas and its impact on PI3K/AKT pathway. *Oncol Rep* **24**, 89–95.

[24] Murayama T, Inokuchi M, Takagi Y, Yamada H, Kojima K, Kumagai J, Kawano T, and Sugihara K (2009). Relation between outcomes and localisation of p_mTOR expression in gastric cancer. *Br J Cancer* **100**, 782–788.

[25] An JY, Kim KM, Choi MG, Noh JH, Sohn TS, Bae JM, and Kim S (2010). Prognostic role of p-mTOR expression in cancer tissues and metastatic lymph nodes in pT2b gastric cancer. *Int J Cancer* **126**, 2904–2913.

[26] Falcon BL, Barr S, Gokhale PC, Chou J, Fogarty J, Depeille P, Miglarese M, Epstein DM, and McDonald DM (2011). Reduced VEGF production, angiogenesis, and vascular regrowth contribute to the antitumor properties of dual mTORC1/mTORC2 inhibitors. *Cancer Research* **71**, 1573–1583.

[27] Guertin DA and Sabatini DM (2007). Defining the role of mTOR in cancer. *Cancer Cell* **12**, 9–22.

[28] Agarwal NK, Chen CH, Cho H, Boulbès DR, Spooner E, and Sarbassov DD (2013). Rictor regulates cell migration by suppressing RhoGDI2. *Oncogene* **32**, 2521–2526.

[29] Wan X, Mendoza A, Khanna C, and Helman LJ (2005). Rapamycin inhibits ezrin-mediated metastatic behavior in a murine model of osteosarcoma. *Cancer Res* **65**, 2406–2411.

[30] Apte SM, Fan D, Killion JJ, and Fidler IJ (2004). Targeting the platelet-derived growth factor receptor in antivascular therapy for human ovarian carcinoma. *Clin Cancer Res* **10**, 897–908.

[31] Kobie K, Kawabata M, Hioki K, Tanaka A, Matsuda H, Mori T, and Maruo K (2007). The tyrosine kinase inhibitor imatinib [STI571] induces regression of xenografted canine mast cell tumors in SCID mice. *Res Vet Sci* **82**, 239–241.

[32] Wolff NC, Veach DR, Tong WP, Bornmann WG, Clarkson B, and Ilaria RL Jr (2005). PD166326, a novel tyrosine kinase inhibitor, has greater antileukemic activity than imatinib mesylate in a murine model of chronic myeloid leukemia. *Blood* **105**, 3995–4003.

[33] Yokoi K, Sasaki T, Bucana CD, Fan D, Baker CH, Kitadai Y, Kuwai T, Abbruzzese JL, and Fidler IJ (2005). Simultaneous inhibition of EGFR, VEGFR, and platelet-derived growth factor receptor signaling combined with gemcitabine produces therapy of human pancreatic carcinoma and prolongs survival in an orthotopic nude mouse model. *Cancer Res* **65**, 10371–10380.

[34] Valiathan RR, Marco M, Leitinger B, Kleer CG, and Fridman R (2012). Discoidin domain receptor tyrosine kinases: new players in cancer progression. *Cancer Metastasis Rev* **31**, 295–321.

[35] Albanell J, Dalmases A, Rovira A, and Rojo F (2007). mTOR signalling in human cancer. *Clin Transl Oncol* **9**, 484–493.

[36] Saunders PO, Weiss J, Welschinger R, Baraz R, Bradstock KF, and Bendall LJ (2013). RAD001 (everolimus) induces dose-dependent changes to cell cycle regulation and modifies the cell cycle response to vincristine. *Oncogene* **32**, 4789–4797.

[37] Guba M, von Breitenbuch P, Steinbauer M, Koehl G, Flegel S, Hornung M, Bruns CJ, Zuelke C, Farkas S, Anthuber M, et al. (2002). Rapamycin inhibits primary and metastatic tumor growth by antiangiogenesis: involvement of vascular endothelial growth factor. *Nat Med* **8**, 128–135.

[38] Bruns CJ, Koehl GE, Guba M, Yezhelyev M, Steinbauer M, Seeliger H, Schwend A, Hoehn A, Jauch KW, and Geissler EK (2004). Rapamycin-induced endothelial cell death and tumor vessel thrombosis potentiate cytotoxic therapy against pancreatic cancer. *Clin Cancer Res* **10**, 2109–2119.

[39] Huber S, Bruns CJ, Schmid G, Hermann PC, Conrad C, Niess H, Huss R, Graeb C, Jauch KW, Heeschen C, et al. (2007). Inhibition of the mammalian target of rapamycin impedes lymphangiogenesis. *Kidney Int* **71**, 771–777.

[40] Kobayashi S, Kishimoto T, Kamata S, Otsuka M, Miyazaki M, and Ishikura H (2007). Rapamycin, a specific inhibitor of the mammalian target of rapamycin, suppresses lymphangiogenesis and lymphatic metastasis. *Cancer Sci* **98**, 726–733.

[41] He Y, Kozaki K, Karpanen T, Koshikawa K, Yla-Herttuala S, Takahashi T, and Alitalo K (2002). Suppression of tumor lymphangiogenesis and lymph node metastasis by blocking vascular endothelial growth factor receptor 3 signaling. *J Natl Cancer Inst* **94**, 819–825.

[42] Zhou HY and Huang SL (2012). Current development of the second generation of mTOR inhibitors as anticancer agents. *Chin J Cancer* **31**, 8–18.